

# Stark effect of shallow impurities in Si

G. D. J. Smit,<sup>\*</sup> S. Rogge,<sup>†</sup> J. Caro, and T. M. Klapwijk

*Department of NanoScience, Delft University of Technology, Lorentzweg 1, 2628 CJ Delft, The Netherlands*

(Dated: August 7, 2021)

We have theoretically studied the effect of an electric field on the energy levels of shallow donors and acceptors in silicon. An analysis of the electric field dependence of the lowest energy states in donors and acceptors is presented, taking the bandstructure into account. A description as hydrogen-like impurities was used for accurate computation of energy levels and lifetimes up to large (several MV/m) electric fields. All results are discussed in connection with atomic scale electronics and solid state quantum computation.

PACS numbers: 71.70.Ej, 71.55.Cn, 03.65.Fd, 03.67.Lx

## I. INTRODUCTION

The field of atomic scale electronics (ASE) aims at controlling charge and spin in semiconductors at the level of *individual* dopant atoms. Such an ability is very attractive, both for physics and for the development of (quantum) devices. From a fundamental point of view, dopant atoms are interesting, because they can be considered as the solid state analogue of atoms in free space. Several well-known effects from atomic physics (e.g. the Stark effect and Zeeman effect) have been studied in great detail in large ensembles of dopant atoms<sup>1</sup>. The prospect of experimentally realizing atomic scale electronics has renewed the interest in dopant atoms. Measurement and control of individual dopant atoms allows for the observation of quantum coherent time evolution and interactions of the dopant's wave functions, which is essential for the operation of a quantum computer.

Manipulation of a single particle's wave functions can be realized by using a local magnetic or electric field. Such a field can be used either to perform the desired manipulation itself, or to provide a local perturbation allowing for addressing a single impurity by a global radiation field. A local electric field could be realized by putting a small gate close to a dopant atom, which is in principle accomplishable with current technology. An ultimate application of gate-manipulation is found in the solid state quantum computer as proposed by Kane<sup>2,3</sup>.

To get more insight in the physics of atomic scale electronic devices, it is essential to try to predict their potential behavior. A first step is the description of isolated dopant atoms in a (homogeneous) electric field. Much more difficult is accurate modelling of a the time evolution of a dopant atom wave function in an inhomogeneous field and the description of the interaction of two or more dopants in a field.

Dopant atoms binding one electron or hole can be described as a hydrogen atom, where the vacuum values of the dielectric constant and the electron mass are replaced by the appropriate values for the semiconductor. This 'scaled hydrogen model' (SHM) provides a reasonable description of the dopant atom's energy levels. Therefore, it is useful to look at existing studies of the Stark effect in the hydrogen atom. Calculation of the shift and

splitting of the hydrogen energy levels up to very large electric field have been carried out by several different methods<sup>4,5,6</sup>. Within the SHM, these results can be directly translated to dopant atoms in a uniform electric field. However, we found that almost no actual results of such calculations in the (field)range of interest for ASE have been published.

The SHM also offers a manageable way to describe a dopant atom in an inhomogeneous electric field. Recently, several calculations using this framework have been published<sup>7,8,9</sup> in the context of quantum computing. However, the SHM fails in the explanation of effects where it is essential that the bandstructure of the semiconductor is taken into account (as an example, see Ref. 10).

Many measurements of the energy levels of dopant atoms in semiconductors (large ensembles) are known, but only a few concerning the effect of a uniform electric field have been reported, presumably because such measurements are much more difficult than e.g. measurements in a magnetic field or under stress. Among them are spectroscopic measurements of the boron energy levels in silicon subject to electric fields up to 0.15 MV/m<sup>11</sup>. Electron-spin-resonance experiments<sup>12</sup> demonstrated that the electric field couples linearly to the acceptor ground state. The magnitude of the effective electric dipole moment for linear Stark coupling has been estimated as 0.26 D for boron acceptors in silicon (1 D =  $3.3 \times 10^{-30}$  Cm). Photo-ionization measurements have shown a very large electric field effect on the phosphorus ground state in Si<sup>13</sup>, but this was measured in highly doped samples where the interaction between dopants dominates the Stark effect of individual energy levels. Finally, quadratic level shifts have been observed in deep selenium double donors in Si, located in the space charge region of a diode<sup>14</sup>.

In this paper, we will theoretically investigate the effect of a uniform electric field on isolated shallow impurities in silicon. Primary interest for ASE will be in the ground state and possibly the first few excited states. These states are the only ones that are well separated from neighboring levels and at low temperatures only the ground state is occupied. Therefore, we focus on the lowest energy states of impurities in silicon. First,

we derive the shift, splitting and wave functions of the lowest donor levels in silicon in a small uniform electric field, taking full account of the multiple valley conduction band structure (Sec. II). We briefly outline a similar calculation for acceptors in silicon (Sec. III). The results are useful for applications where a local gate is used to bring a single dopant atom into resonance with a global radiation field (nuclear magnetic resonance, electron spin resonance). Moreover, they can be used to outline the limitations of the SHM. Second, in Sec. IV we present accurate numerical calculation of the Stark effect in silicon within SHM, from zero field up to fields that are relevant for atomic scale electronics and quantum computing (several MV/m; see for instance Ref. 3). Finally, we conclude by discussing possible extensions and alternatives of our methods which are useful to address issues in ASE (Sec. V).

## II. DONORS

### A. The donor ground state

Group theory is a powerful tool to derive various properties of dopant wave functions in a semiconductor. In order to provide the necessary background and to fix the notation, we will briefly review some relevant properties of donor levels in silicon (see e.g. Ref. 15). Degeneracy due to spin is not lifted by an electric field in donors. For simplicity, we will therefore not count those degeneracies in this section.

The conduction band of silicon has six equivalent minima located on the  $[100]$  and equivalent axes. These minima are commonly called ‘valleys’ and we label them by the numbers 1 to 6 as shown in Fig. 1(a). The band structure in the vicinity of valley 1, located in  $k$ -space at  $\mathbf{k}_1 = (k_0, 0, 0)$ , can be approximated as

$$E = E_0 + \frac{\hbar^2}{2m_{\parallel}}(k_x - k_0)^2 + \frac{\hbar^2}{2m_{\perp}}(k_y^2 + k_z^2),$$

where  $m_{\parallel} = 0.98m$  and  $m_{\perp} = 0.19m$  are the electron effective masses and  $m$  is the free electron mass. Furthermore,  $k_0 = 0.85 \frac{2\pi}{a}$ , where  $a$  is the size of the silicon unit cell. Similar expressions hold for the remaining five valleys.

From effective mass theory (EMT) it follows that the ground state wave function of the Hamiltonian of an electron bound to a donor can be written as<sup>17</sup>

$$\Psi(\mathbf{r}) = \sum_{\mu=1}^6 \alpha_{\mu} F_{\mu}(\mathbf{r}) \varphi_{\mu}(\mathbf{r}), \quad (1)$$

where the  $\alpha_{\mu}$  are numerical coefficients and the  $F_{\mu}(\mathbf{r})$  are envelope wave functions, which are slowly varying on the length scale of  $a$ .  $F_1(\mathbf{r}) = F_2(\mathbf{r})$  satisfy the hydrogen-like

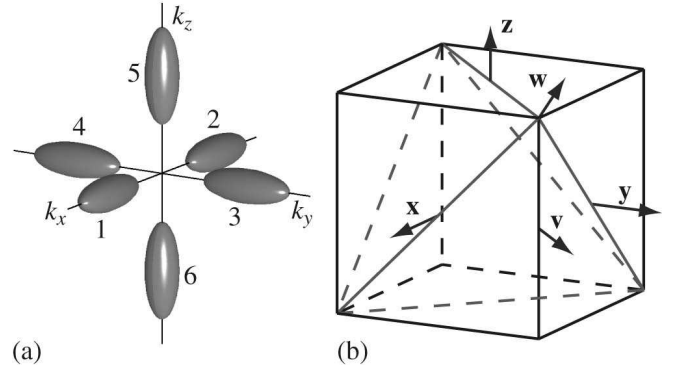


FIG. 1: (a) Schematic representation of the conduction band valleys of silicon as constant energy surfaces in  $k$ -space. The six valleys are labelled by numbers, e.g. 4 represents the  $[0\bar{1}0]$  valley. (b) Definition of the coordinate system with respect to the Si-crystal unit cell. We have  $\mathbf{x} \parallel [100]$ ,  $\mathbf{y} \parallel [010]$ ,  $\mathbf{z} \parallel [001]$ ,  $\mathbf{v} \parallel [110]$ , and  $\mathbf{w} \parallel [111]$ . The orientation of the figure in part (a) and (b) is the same.

Schrödinger equation

$$-\left[ \frac{\hbar^2}{2m_{\parallel}} \frac{\partial^2}{\partial x^2} + \frac{\hbar^2}{2m_{\perp}} \left( \frac{\partial^2}{\partial y^2} + \frac{\partial^2}{\partial z^2} \right) + \frac{e^2}{4\pi\epsilon r} \right] F(\mathbf{r}) = E F(\mathbf{r}) \quad (2)$$

and similar equations hold for the remaining  $F_{\mu}$ . The  $\varphi_{\mu}(\mathbf{r})$  are Bloch-wave functions at the minimum of valley  $\mu$  and can be written as  $e^{i\mathbf{k}_{\mu} \cdot \mathbf{r}} u_{\mu}(\mathbf{r})$ , where  $u_{\mu}(\mathbf{r})$  has the periodicity of the silicon crystal lattice. Because for all  $\mu$  the eigenvalues resulting from Eq. (2) are the same, Eq. (1) shows that the degeneracy of each of these eigenvalues is multiplied by six for the total wave functions  $\Psi(\mathbf{r})$ . In particular, the ground state solution of Eq. (2) gives rise to a six-fold degenerate donor ground state.

The symmetry group of the conduction band minima (and thus of the Bloch functions  $\varphi(\mathbf{r})$ ) is  $C_{\infty v}$  in EMT, which reduces to  $C_{2v}$  in the silicon crystal. The envelope wave functions  $F(\mathbf{r})$  belong to  $D_{\infty h}$ . Their products belong to the cross-section of both groups, which is  $C_{2v}$ . For the  $1s$ -like ( $m = 0$ ) ground state function of Eq. 2  $F_{\mu}(\mathbf{r})$ , such a product transforms according to the  $\Gamma_1$  representation of the valley symmetry group  $C_{2v}$ . Because the donor is located at a substitutional site of the tetrahedral silicon lattice, the total wave function has  $T_d$ -symmetry. Using Frobenius' theorem<sup>18</sup>, it can be shown that the  $\Gamma_1$  representation of  $C_{2v}$  induces the  $\Gamma_1 + \Gamma_3 + \Gamma_5$  representation<sup>30</sup> of  $T_d$ . This means that linear combinations of the  $F_{\mu}(\mathbf{r})$  can be found that have the correct transformation properties under  $T_d$ . Using the notation  $\boldsymbol{\alpha} = (\alpha_1, \dots, \alpha_6)$  (as in Eq. 1) the reduction to the  $T_d$

representations is carried out by

$$\begin{aligned}
 \alpha_g &= \frac{1}{\sqrt{6}}(1, 1, 1, 1, 1) & \Gamma_1 \\
 \alpha_r &= \frac{1}{\sqrt{12}}(-1, -1, -1, -1, 2, 2) \\
 \alpha_s &= \frac{1}{2}(1, 1, -1, -1, 0, 0) & \left. \vphantom{\begin{matrix} \alpha_r \\ \alpha_s \end{matrix}} \right\} \Gamma_3 \\
 \alpha_x &= \frac{1}{\sqrt{2}}(1, -1, 0, 0, 0, 0) \\
 \alpha_y &= \frac{1}{\sqrt{2}}(0, 0, 1, -1, 0, 0) & \left. \vphantom{\begin{matrix} \alpha_x \\ \alpha_y \end{matrix}} \right\} \Gamma_5 \\
 \alpha_z &= \frac{1}{\sqrt{2}}(0, 0, 0, 0, 1, -1)
 \end{aligned} \tag{3}$$

Each of the vectors  $\alpha$  defines a wave function  $\Psi$  through Eq. 1. Here, the basis functions of the two- and three dimensional representations have been chosen such that  $\Psi_r$  and  $\Psi_s$  transform under  $T_d$  as  $3z^2 - r^2$  and  $\sqrt{3}(x^2 - y^2)$ , respectively. Similarly,  $\Psi_x$ ,  $\Psi_y$  and  $\Psi_z$  have been chosen such that they transform under  $T_d$  as  $x$ ,  $y$  and  $z$ , respectively.

The potential term in the EMT-Schrödinger equation (2) is a good approximation only for  $r \gtrsim a$ , where  $a$  is the lattice constant of silicon. For small  $r$ , the charge of the nucleus is not screened by other electrons and it will attract electrons much stronger than described by the potential in Eq. (2). Because the symmetry of the potential is not affected, the states are still described by the representations of  $T_d$ , but they are no longer degenerate. The  $\Gamma_1$  state  $\Psi_g$  is the only one of the six ground state wave functions that has non-zero electron density at the nucleus ( $\mathbf{r} = 0$ ). Therefore, it has a larger binding energy than predicted by EMT and for most donors in silicon the  $1s(\Gamma_1)$  state is the true ground state. This effect is generally called ‘chemical splitting’ (because the size of the effect depends on the donor in question) or ‘valley-orbit splitting’. The remaining states (especially the non- $s$  states) are quite well described by EMT, because the electron density at the nucleus is negligible. As an example, in case of phosphorus in silicon, the  $1s(\Gamma_1)$  state (the ground state) has been measured to be located 45.29 meV below the conduction band minimum<sup>1</sup>, while the EMT-prediction is 31.27 meV<sup>19</sup>.

### B. Symmetry of the donor ground state in an electric field

After this brief review of established knowledge of silicon donors, we return to the main subject of this paper. From purely symmetry based considerations, we can find how the Hilbert subspace spanned by the original six valley wave functions is decomposed by the application of an electric field in a certain direction. The impurities considered in this paper occupy substitutional sites in the silicon lattice and their wave functions transform according to representations of site symmetry group  $\bar{T}_d$ . The symmetry group of a uniform electric field  $\mathcal{E}$  is  $C_{\infty v}$ . When  $\mathcal{E}$  is applied in an arbitrary direction in the silicon crystal, the symmetry group  $\bar{T}_d$  of the Hamiltonian reduces to the trivial group  $C_1$ . Only when the direction

TABLE I: Reduction of the site symmetry of an impurity in a uniform electric field in various directions and the resulting reduction of the irreducible representations<sup>20</sup>.

Direction	$\langle 100 \rangle$	$\langle 111 \rangle$	$\langle 110 \rangle$
Group	$\bar{C}_{2v}$	$\bar{C}_{3v}$	$\bar{C}_s$
$\Gamma_1 (\bar{T}_d)$	$\Gamma_1$	$\Gamma_1$	$\Gamma_1$
$\Gamma_2 (\bar{T}_d)$	$\Gamma_3$	$\Gamma_2$	$\Gamma_2$
$\Gamma_3 (\bar{T}_d)$	$\Gamma_1 + \Gamma_3$	$\Gamma_3$	$\Gamma_1 + \Gamma_2$
$\Gamma_4 (\bar{T}_d)$	$\Gamma_2 + \Gamma_3 + \Gamma_4$	$\Gamma_2 + \Gamma_3$	$\Gamma_1 + 2\Gamma_2$
$\Gamma_5 (\bar{T}_d)$	$\Gamma_1 + \Gamma_2 + \Gamma_4$	$\Gamma_1 + \Gamma_3$	$2\Gamma_1 + \Gamma_2$
$\Gamma_6 (\bar{T}_d)$	$\Gamma_5$	$\Gamma_4$	$\Gamma_{3+4}$
$\Gamma_7 (\bar{T}_d)$	$\Gamma_5$	$\Gamma_4$	$\Gamma_{3+4}$
$\Gamma_8 (\bar{T}_d)$	$2\Gamma_5$	$\Gamma_4 + \Gamma_{5+6}$	$2\Gamma_{3+4}$

of the field is along one of the main crystallographic directions of the crystal, the result is  $C_{2v}$  for  $\mathcal{E} \parallel \langle 100 \rangle$ ,  $C_{3v}$  for  $\mathcal{E} \parallel \langle 111 \rangle$ , and  $C_s$  for  $\mathcal{E} \parallel \langle 110 \rangle$ . The reduction of symmetry can induce a splitting in the original energy levels as shown in Table I. As expected, the electric field does not remove degeneracy due to time reversal symmetry and therefore all resulting levels are at least two-fold degenerate.

To make the connection to the valley wave functions  $F_\mu(\mathbf{r})\phi_\mu(\mathbf{r})$ , we will now discuss the symmetry of the  $1s$  levels in an electric field from another point of view. We start by looking at the individual valley wave functions and subsequently derive which linear combinations form appropriate donor wave functions (using the method of Ref. 21). When a donor impurity in silicon is situated in an electric field along the positive  $z$ -direction, the valleys 5 and 6 keep their  $C_{2v}$  symmetry, while the field reduces the symmetry group of the other four valleys to  $C_1$ . These four valleys are mixed by the elements of the site symmetry group  $C_{2v}$  and are therefore grouped together in the third column of Table II.

In case of a  $1s$  state, the valley wave functions belong to the  $\Gamma_1$  representation of  $C_{2v}$  (for valley 5 and 6) or  $C_1$  (for 1, 2, 3 and 4). This is found by reducing the even  $m = 0$  representation of  $D_{\infty h}$  to  $C_{2v}$  and  $C_1$ , respectively. By using Frobenius’ theorem, it can be deduced that these generate for the impurity wave function the representations  $\Gamma_1$  and  $\Gamma_1 + \Gamma_2 + \Gamma_3 + \Gamma_4$  of  $C_{2v}$ , respectively. This is also shown in Table II, together with the (set of) induced wave function(s) spanning the subspace of that representation. In a similar way, we obtained results for the electric field in the other main crystallographic directions. They are also shown in the table.

Due to the valley-orbit splitting (which has been ignored so far) the three irreducible components of the donor ground state are already energetically separated at zero field. Therefore, the basis vectors have to be chosen in such a way that they agree with the zero-field energy splitting of the  $\Gamma_1$ ,  $\Gamma_3$  and  $\Gamma_5$  levels of  $T_d$ <sup>31</sup>. The result for various directions of the electric field is shown in Table III.

TABLE II: Considering the symmetry of the valley wave functions in an electric field, the symmetry of the total wave function they induce can be obtained. The results for the 1s level, without considering valley-orbit splitting, are shown in this table. The direction of  $\mathcal{E}$  in the first column is denoted by the vectors defined in Fig. 1(a). The fifth column lists the representations of the appropriate site symmetry group, given in the second column. The basis vectors are given in the notation of Eq. (3).

Dir.	Site	Valley	Valley	$\Gamma(\text{site})$	Basis
$\mathcal{E}$	sym.		sym.		
$\mathbf{z}$	$C_{2v}$	1, 2, 3, 4	$C_1$	$\Gamma_1$	(1, 1, 1, 1, 0, 0)
				$\Gamma_2$	(1, -1, 1, -1, 0, 0)
				$\Gamma_3$	(1, 1, -1, -1, 0, 0)
				$\Gamma_4$	(1, -1, -1, 1, 0, 0)
	5	$C_{2v}$	$\Gamma_1$	(0, 0, 0, 0, 1, 0)	
				(0, 0, 0, 0, 0, 1)	
	$C_{3v}$	1, 3, 5	$C_s$	$\Gamma_1$	(1, 0, 1, 0, 1, 0)
				$\Gamma_3$	( $\omega^2, 0, \omega, 0, 1, 0$ )
					( $\omega, 0, \omega^2, 0, 1, 0$ )
				$\Gamma_1$	(0, 1, 0, 1, 0, 1)
	2, 3, 6	$C_s$	$\Gamma_3$	(0, $\omega^2, 0, \omega, 0, 1$ )	
				(0, $\omega, 0, \omega^2, 0, 1$ )	
$\mathbf{v}$	$C_s$	1, 3	$C_1$	$\Gamma_1$	(1, 0, 1, 0, 0, 0)
				$\Gamma_2$	(1, 0, -1, 0, 0, 0)
	2, 4	$C_1$	$\Gamma_1$	(0, 1, 0, 1, 0, 0)	
				$\Gamma_2$	(0, 1, 0, -1, 0, 0)
	5	$C_s$	$\Gamma_1$	(0, 0, 0, 0, 1, 0)	
				(0, 0, 0, 0, 0, 1)	
	6	$C_s$	$\Gamma_1$	(0, 0, 0, 0, 0, 1)	
				(0, 0, 0, 0, 0, 1)	

### C. Shift and splitting in an electric field

Now, we will derive the shift and splitting of the lowest donor levels in an electric field from a perturbation calculation. Results for other levels can be derived using the same method, although (because the level spacing is smaller for higher levels) the range of fields where the perturbation calculation is valid is much smaller.

Although the six-fold degeneracy of the 1s-levels is lifted by the valley orbit interaction, the complete manifold is relatively well-separated from the higher levels (the separation of the highest 1s( $\Gamma_3$ ) level to closest excited level ( $2p_0$ ) is roughly twice as large as the separation between the 1s( $\Gamma_1$ ) and 1s( $\Gamma_3$ ) levels). Therefore, we consider the 1s-manifold as a whole in a single perturbation calculation, taking only the coupling among the 1s levels themselves into account.

The electric field couples to the (induced) dipole moment  $\mathbf{D} = e\mathbf{r}$  of the impurity state and gives rise to an additional term in its Hamiltonian  $-\mathcal{E} \cdot \mathbf{D}$ , reflecting the energy associated with the dipole in the field. By mak-

ing use of the Wigner-Eckart orthogonality theorem from group theory<sup>22</sup>, it is possible to find the vanishing matrix elements as well as the dependencies between the non-vanishing matrix elements, as they follow from the symmetry of the system. The 1s sub-matrix  $[\mathcal{H}]$  of the total Stark Hamiltonian  $\mathcal{H} = \mathcal{H}_0 + \mathcal{E} \cdot \mathbf{D}$  is given by

$$\begin{pmatrix} E_1 & 0 & 0 & p_{15}\mathcal{E}_x & p_{15}\mathcal{E}_y & p_{15}\mathcal{E}_z \\ 0 & E_3 & 0 & -p_{35}\mathcal{E}_x & -p_{35}\mathcal{E}_y & 2p_{35}\mathcal{E}_z \\ 0 & 0 & E_3 & p_{35}\sqrt{3}\mathcal{E}_x & -p_{35}\sqrt{3}\mathcal{E}_y & 0 \\ \bar{p}_{15}\mathcal{E}_x & -\bar{p}_{35}\mathcal{E}_x & \bar{p}_{35}\sqrt{3}\mathcal{E}_x & E_5 & p_5\mathcal{E}_z & p_5\mathcal{E}_y \\ \bar{p}_{15}\mathcal{E}_y & -\bar{p}_{35}\mathcal{E}_y & \bar{p}_{35}\sqrt{3}\mathcal{E}_y & \bar{p}_5\mathcal{E}_z & E_5 & p_5\mathcal{E}_x \\ \bar{p}_{15}\mathcal{E}_z & 2\bar{p}_{35}\mathcal{E}_z & 0 & \bar{p}_5\mathcal{E}_y & \bar{p}_5\mathcal{E}_x & E_5 \end{pmatrix}.$$

The elements of this matrix are given by  $[\mathcal{H}]_{ij} = \langle \varphi_i | \mathcal{H} | \varphi_j \rangle$ , where the wave functions  $\varphi_i$  are taken from the basis  $(\Psi_g, \Psi_r, \Psi_s, \Psi_x, \Psi_y, \Psi_z)$  as defined before. The energies  $E_1$ ,  $E_3$  and  $E_5$  are the eigenvalues of the unperturbed Hamiltonian  $\mathcal{H}_0$ , that is the zero-field energies of the 1s( $\Gamma_1$ ), 1s( $\Gamma_3$ ) and 1s( $\Gamma_5$ ) level, respectively. For phosphorous in silicon, the values are  $E_1 = -45.59$  meV,  $E_3 = -32.58$  meV, and  $E_5 = -33.89$  meV with respect to the conduction band edge<sup>1</sup>. The parameters  $p_{15}$ ,  $p_{35}$  and  $p_5$  describe the coupling between the 1s-levels. As can be seen, these are the only three independent parameters describing the coupling between the levels. They can be expressed in terms of integrals over products of wave functions, e.g.  $p_{15} = e\langle \Psi_g | x | \Psi_x \rangle$  and  $p_5 = e\langle \Psi_y | x | \Psi_z \rangle$ .

Perturbation theory is invoked by calculating the eigenvalues and eigenvectors of this  $6 \times 6$  matrix up to second order in  $\mathcal{E}$ . This yields the 1s energy levels and wave functions as a function of electric field for  $\mathcal{E}$  along the three main crystallographic directions. The energy levels are presented in the last column of Table III. From Table III it can be seen that the 1s( $\Gamma_1$ ) ground state experiences an isotropic quadratic shift downwards<sup>32</sup>, while for the other levels the behavior depends on the direction of the electric field. In Figure 2 the results for  $\mathcal{E} \parallel \langle 100 \rangle$  are plotted schematically.

The corresponding eigenvectors were also obtained from this calculation. In the limit  $\mathcal{E} \rightarrow 0$  they coincide with the vectors given in Table III, allowing to label each eigenvalue with the correct representation. These results are directly applicable in the prediction of allowed optical transitions between the various levels.

We discuss the behavior of the three 1s states in in some more detail. The normalized eigenfunctions in an electric field parallel to  $\mathbf{z}$  (again up to second order in  $\mathcal{E}$ ) corresponding to the eigenvalues already given in Ta-

TABLE III: Reduction of the 1s donor energy levels in an electric field. The basis vectors belonging to these states are given (in the notation of Eq. (3)) in the limit  $\mathcal{E} \rightarrow 0$  ( $\omega = e^{2\pi i/3}$ ). The eigenvalues (up to second order in  $\mathcal{E}$ ) are the result of the perturbation calculation described in the text.

Field direction	$\mathcal{E} = 0$	$\mathcal{E} \neq 0$	Basis vector(s)	Eigenvalue
<b>z</b>	$\Gamma_1(T_d)$	$\Gamma_1(C_{2v})$	$(1, 1, 1, 1, 1, 1)/\sqrt{6}$	$E_1 - \frac{ p_{15} ^2}{E_5 - E_1} \mathcal{E}^2$
	$\Gamma_3(T_d)$	$\Gamma_1(C_{2v})$	$(1, 1, 1, 1, -2, -2)/\sqrt{12}$	$E_3 + \frac{ 2p_{35} ^2}{E_3 - E_1} \mathcal{E}^2$
		$\Gamma_3(C_{2v})$	$(1, 1, -1, 1, 0, 0)/2$	$E_3$
	$\Gamma_5(T_d)$	$\Gamma_1(C_{2v})$	$(0, 0, 0, 0, 1, -1)/\sqrt{2}$	$E_5 + (\frac{ p_{15} ^2}{E_5 - E_1} + \frac{ 2p_{35} ^2}{E_3 - E_1}) \mathcal{E}^2$
<b>w</b>		$\Gamma_2(C_{2v})$	$(1, -1, 1, -1, 0, 0)/\sqrt{2}$	$E_5 +  p_5  \mathcal{E}$
		$\Gamma_4(C_{2v})$	$(1, -1, -1, 1, 0, 0)/\sqrt{2}$	$E_5 -  p_5  \mathcal{E}$
	$\Gamma_1(T_d)$	$\Gamma_1(C_{3v})$	$(1, 1, 1, 1, 1, 1)/\sqrt{6}$	$E_1 - \frac{ p_{15} ^2}{E_5 - E_1} \mathcal{E}^2$
	$\Gamma_3(T_d)$	$\Gamma_3(C_{3v})$	$(\omega^2, \omega^2, \omega, \omega, 1, 1)/\sqrt{6}$ $(\omega, \omega, \omega^2, \omega^2, 1, 1)/\sqrt{6}$	$E_3 + \frac{2 p_{35} ^2}{E_3 - E_5} \mathcal{E}^2$
<b>v</b>	$\Gamma_5(T_d)$	$\Gamma_1(C_{3v})$	$(1, -1, 1, -1, 1, -1)/\sqrt{6}$	$E_5 \pm \frac{2}{3}\sqrt{3} p_5  \mathcal{E} + (\frac{ p_{15} ^2}{E_5 - E_1} - \frac{4 p_{35} ^2}{E_3 - E_5}) \mathcal{E}^2$
		$\Gamma_3(C_{3v})$	$(\omega^2, -\omega^2, \omega, -\omega, 1, -1)/\sqrt{6}$ $(\omega, -\omega, \omega^2, -\omega^2, 1, -1)/\sqrt{6}$	$E_5 \mp \frac{1}{3}\sqrt{3} p_5  \mathcal{E}$
	$\Gamma_1(T_d)$	$\Gamma_1(C_s)$	$(1, 1, 1, 1, 1, 1)/\sqrt{6}$	$E_1 - \frac{ p_{15} ^2}{E_5 - E_1} \mathcal{E}^2$
	$\Gamma_3(T_d)$	$\Gamma_1(C_s)$	$(1, 1, 1, 1, -2, -2)/\sqrt{12}$	$E_3 + \frac{ p_{35} ^2}{E_3 - E_1} \mathcal{E}^2$
<b>v</b>		$\Gamma_2(C_s)$	$(1, 1, -1, 1, 0, 0)/2$	$E_3 + \frac{3 p_{35} ^2}{E_3 - E_1} \mathcal{E}^2$
	$\Gamma_5(T_d)$	$\Gamma_1(C_s)$	$(0, 0, 0, 0, 1, -1)/\sqrt{2}$	$E_5 +  p_5  \mathcal{E} - \frac{1}{2}(\frac{ p_{35} ^2}{E_3 - E_1} - \frac{ p_{15} ^2}{E_5 - E_1}) \mathcal{E}^2$
		$\Gamma_1(C_s)$	$(1, -1, 1, -1, 0, 0)/\sqrt{2}$	$E_5 -  p_5  \mathcal{E} - \frac{1}{2}(\frac{ p_{35} ^2}{E_3 - E_1} - \frac{ p_{15} ^2}{E_5 - E_1}) \mathcal{E}^2$
		$\Gamma_2(C_s)$	$(1, -1, -1, 1, 0, 0)/\sqrt{2}$	$E_5 - \frac{3 p_{35} ^2}{E_3 - E_1} \mathcal{E}^2$

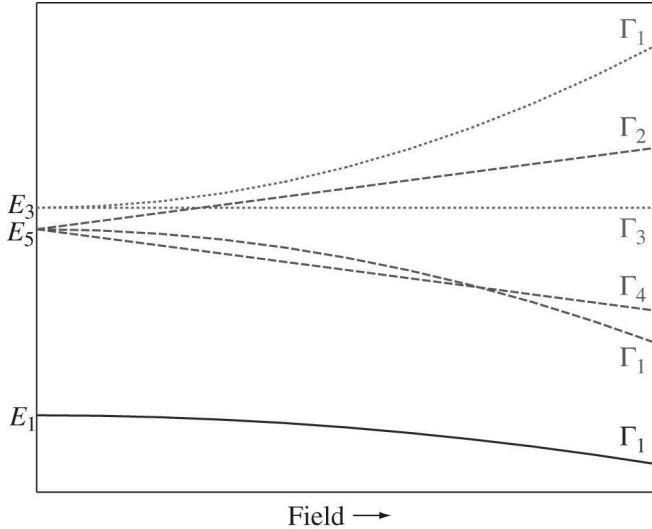


FIG. 2: Schematic plot of the 1s energy levels as a function of the electric field  $\mathcal{E}$ . The values of the parameters  $p_5$ ,  $p_{15}$ , and  $p_{35}$  have been chosen such that the plot clearly illustrates the qualitative features of the Stark effect in the energy levels.

ble III are

$$\begin{aligned}
 \Phi_g &= (1 - \frac{1}{2}|\beta|^2 \mathcal{E}^2) \Psi_g + \beta'' \mathcal{E}^2 \cdot \Psi_r - \bar{\beta} \mathcal{E} \cdot \Psi_z \\
 \Phi_r &= -\bar{\beta}'' \mathcal{E}^2 \cdot \Psi_g + (1 - \frac{1}{2}|\beta'|^2 \mathcal{E}^2) \Psi_r + \bar{\beta}' \mathcal{E} \cdot \Psi_z \\
 \Phi_s &= \Psi_s \\
 \Phi_x &= \frac{1}{2}\sqrt{2}(\Psi_x + \Psi_y) \\
 \Phi_y &= \frac{1}{2}\sqrt{2}(\Psi_x - \Psi_y) \\
 \Phi_z &= \beta \mathcal{E} \cdot \Psi_g - \beta' \mathcal{E} \cdot \Psi_r + \\
 &\quad (1 - \frac{1}{2}(|\beta|^2 + |\beta'|^2) \mathcal{E}^2) \Psi_z
 \end{aligned} \tag{4}$$

where

$$\beta = \frac{p_{15}}{E_5 - E_1}, \quad \beta' = \frac{2p_{35}}{E_3 - E_5}, \quad \beta'' = \bar{\beta} \frac{2p_{35}}{E_3 - E_1}.$$

The initial zero field wave function  $\Psi_g$  has the highest spacial symmetry possible in a tetrahedral lattice. To get more insight in the contribution of the six valleys as a function of the applied field, we can write the perturbed ground state wave function  $\Phi_g$  in the notation of Eq. (3)

as

$$(1, 1, 1, 1, 1, 1) + (0, 0, 0, 0, -\gamma'', \gamma'')\mathcal{E} + (-\gamma, -\gamma, -\gamma, -\gamma, -\gamma', -\gamma')\mathcal{E}^2,$$

where

$$\gamma = \frac{1}{2}(|\beta|^2 + \beta''\sqrt{2}), \quad \gamma' = \frac{1}{2}(|\beta|^2 - 2\beta''\sqrt{2}), \quad \gamma'' = \bar{\beta}\sqrt{3}$$

and an overall factor  $1/\sqrt{6}$  was omitted. From these expressions, we see that the contribution of the valley in the  $-\mathbf{z}$  direction increases linearly with the field, while contribution of the opposite valley decreases linearly with the field. This reflects the field-induced dipole moment of the ground state.

The results of this calculation could be made quantitative if the values of the parameters  $p_5$ ,  $p_{15}$ , and  $p_{35}$  were known. This can be done by evaluating the integrals defining these parameters and using e.g. the EMT wave functions from Eq. (1). However, due to the strongly oscillating integrands, this is numerically a non-trivial task. Furthermore, the EMT wave functions have a higher symmetry than the lattice, and the value for  $p_5$  obtained in this way is always zero. An estimate for  $p_5$  can only be obtained using more sophisticated approximations for the wave functions. More importantly, the applicability of such results is limited, especially for the  $1s$  state, as the effects of valley-orbit interaction are not included in the EMT wave functions.

It is important to note that the energies in Table III and the eigenstates in Eq. (4) are based on symmetry properties only and not on the explicit form of the EMT wave functions. Therefore, these results remain valid, even if valley-orbit interaction and central cell corrections are fully included. Such modifications would only influence the values of the parameters  $p_5$ ,  $p_{15}$ , and  $p_{35}$ .

### III. ACCEPTORS

Acceptor wave functions can be equally well used for ASE as donors. Recent experiments showing that the coherence time of spins of bound holes is more than 1 ms<sup>23</sup>, even justify the prospective use of acceptor wave functions as qubits. We therefore also briefly outline the properties of silicon acceptors in an electric field, taking the silicon valence band structure into account. The initially threefold degenerate valence band maximum is split by spin orbit interaction, which causes one of the bands to shift downwards by  $\sim 43$  meV<sup>1</sup>. Due to the spin-orbit interaction, spin is not a good quantum number anymore and the bands must be characterized by the total angular momentum, which is  $\frac{3}{2}$  for the upper two bands. Due to the half-valued angular momentum, the Bloch wave function at the valence band maximum transforms according to one of the double valued representations of  $\bar{T}_d$ , namely  $\Gamma_8$ . As a result, the total impurity wave functions transform according to representations of the same group. The

ground state wave function, as well as the first few excited levels belong to the  $\Gamma_8$  representation and they are all four-fold degenerate (including spin).

#### A. Linear Stark effect

To derive the small-field splitting of acceptors in silicon in an electric field, we use degenerate perturbation theory for each level individually. To that end, the Hamiltonian sub-matrix  $\langle \varphi_i | \mathcal{H} | \varphi_j \rangle$  of the level under consideration must be calculated and diagonalized, where the  $\varphi_i$  form a suitable basis for the subspace of that particular level.

As mentioned before, the components of the electric dipole operator  $e\mathbf{r}$  transform according to the rows of the  $\Gamma_5$  representation of  $\bar{T}_d$ . Because the anti-symmetrized direct products  $\{\Gamma_6 \times \Gamma_6\} = \{\Gamma_7 \times \Gamma_7\} = \Gamma_1$  do not contain  $\Gamma_5$ , the first order Stark matrix vanishes for levels with  $\Gamma_6$  or  $\Gamma_7$  symmetry. Hence, such levels do not experience a linear Stark effect. On the other hand,  $\{\Gamma_8 \times \Gamma_8\} = \Gamma_1 + \Gamma_3 + \Gamma_5$  does contain  $\Gamma_5$ , so that a linear Stark effect is possible for a  $\Gamma_8$  level<sup>33</sup>.

The effective linear Stark Hamiltonian<sup>34</sup> for a  $\Gamma_8$  level is given by<sup>24</sup>

$$[\mathcal{H}]_8^{\text{lin}} = \frac{2}{\sqrt{3}}p_8(\mathcal{E}_x\{J_y, J_z\} + \mathcal{E}_y\{J_z, J_x\} + \mathcal{E}_z\{J_x, J_y\}),$$

where the parameter  $p_8$  is related to the effective dipole moment of such a state. The  $J_i$  ( $i = x, y, z$ ) are matrices of the components of the angular momentum operator with respect to some convenient basis and  $\{A, B\} = \frac{1}{2}(AB + BA)$  is the anti-commutator. The eigenvalues of this matrix are given by

$$E_8 \pm |p_8|\mathcal{E},$$

where both eigenvalues occur twice. This is a symmetric splitting of the level, which is independent of the direction of  $\mathcal{E}$ . Note that  $p_8$  vanishes within EMT, similar to  $p_5$  before. Estimates of  $p_8$  obtained in literature range from  $10^{-2}$  D<sup>24</sup> to 0.26 D<sup>12</sup>.

#### B. Quadratic Stark effect

Because  $\{\Gamma_6 \times \Gamma_6\} = \{\Gamma_7 \times \Gamma_7\} = \Gamma_1$ , the quadratic effective Stark-Hamiltonian for a  $\Gamma_6$  and  $\Gamma_7$  level is simply given by

$$\mathcal{H}_{\text{eff,quad}} = a_i\mathcal{E}^2\hat{I},$$

where  $\hat{I}$  is the identity matrix and the  $a_i$  ( $i = 6, 7$ ) are phenomenological parameters, that can be expressed in terms of integrals over wave functions. It follows that the  $\Gamma_6$  and  $\Gamma_7$  levels experience an isotropic quadratic shift

$$E_i + a_i\mathcal{E}^2,$$

where  $E_i$  is the unperturbed energy of a  $\Gamma_i$  level. The two-fold degeneracy due to time reversal symmetry is obviously not removed by the electric field.

The quadratic part of the effective Hamiltonian for a  $\Gamma_8$  level, such as the ground state, is given by<sup>24</sup>

$$[\mathcal{H}]_8^{\text{quad}} = a_8 \mathcal{E}^2 \hat{I} + b_8 [J_x^2 \mathcal{E}_x^2 + J_y^2 \mathcal{E}_y^2 + J_z^2 \mathcal{E}_z^2 - \frac{1}{3} \mathbf{J}^2] + \frac{2}{\sqrt{3}} c_8 [\{J_x, J_y\} \mathcal{E}_x \mathcal{E}_y + \{J_y, J_z\} \mathcal{E}_y \mathcal{E}_z + \{J_z, J_x\} \mathcal{E}_z \mathcal{E}_x],$$

where  $a_8$ ,  $b_8$  and  $c_8$  are again phenomenological parameters. The total Hamiltonian has two distinct eigenvalues

$$a_8 \mathcal{E}^2 \pm [p^2 \mathcal{E}^2 + b_8^2 \mathcal{E}^4 + (c_8^2 - 3b_8^2)(\mathcal{E}_y^2 \mathcal{E}_z^2 + \mathcal{E}_x^2 \mathcal{E}_z^2 + \mathcal{E}_x^2 \mathcal{E}_y^2) + 6p_8 c_8 \mathcal{E}_x \mathcal{E}_y \mathcal{E}_z]^{1/2}, \quad (5)$$

each of which is still doubly degenerate (due to time reversal symmetry)<sup>35</sup>. For  $\mathcal{E} \parallel \langle 100 \rangle$  this expression reduces to (up to second order in  $\mathcal{E}$ )

$$E_8 \pm |p_8| \mathcal{E} + a_8 \mathcal{E}^2.$$

For  $\mathcal{E} \parallel \langle 111 \rangle$  we find

$$E_8 \pm |p_8| \mathcal{E} + (a_8 \pm \frac{1}{3} \sqrt{3} c_8) \mathcal{E}^2$$

and for  $\mathcal{E} \parallel \langle 110 \rangle$  we have

$$E_8 \pm |p_8| \mathcal{E} + a_8 \mathcal{E}^2.$$

The results for  $\mathcal{E} \parallel \langle 100 \rangle$  and for  $\mathcal{E} \parallel \langle 110 \rangle$  are the same in this approximation, but different in third order.

Obviously, the wave functions of donors and acceptors are very different and this is reflected in their respective electric field behavior. The donor ground state undergoes an isotropic quadratic shift. The acceptor ground state has an isotropic linear splitting, superposed on an anisotropic quadratic shift.

In the spectroscopic measurements of boron acceptors in silicon<sup>11</sup> (mentioned in the introduction), the observed  $\Gamma_8$ -levels indeed show a quadratic shift. However, the expected level-splitting was not observed, most likely due to limited resolution.

#### IV. LARGE ELECTRIC FIELDS IN SHM

In this section, we will calculate energy levels of an impurity in a semiconductor as a function of electric field in the range from zero to  $\sim 5$  MV/m. This is done within the scaled hydrogen model, where the band structure of the semiconductor is accounted for by a single effective mass and the dielectric constant only.

For this calculation it is convenient to express all quantities in so-called effective atomic units. For instance,

TABLE IV: Atomic units for some relevant physical quantities in vacuum and silicon. For silicon the values  $\varepsilon_s = 11.4$  and  $m^* = 0.26$  (appropriate for electrons) were taken.

Quantity	Unit	Value in vacuum	Value in Si
Energy	2Ry	27.2 eV	54 meV
Length	$a_0$	0.053 nm	2.3 nm
Electric field	2Ry/ $ea_0$	510 GV/m	24 MV/m
Time	$\hbar/2\text{Ry}$	$2.4 \cdot 10^{-17}$ s	$1.2 \cdot 10^{-14}$ s

energies are expressed in units of twice the effective ionization energy and length in units of the effective Bohr-radius. Conversion of units of relevant quantities for both vacuum and silicon are given in Table IV.

In the past, several algorithms have been described in literature to calculate electric field dependence of the energy levels of the hydrogen atom. However, very little results in the range of interest for ASE (fields up to  $\sim 0.1$  a.u.<sup>3</sup>) have been published. Therefore, we found it important to fill this gap by fully presenting the results of our calculation. For this purpose, we used the slightly adapted version of a variational algorithm that not only yields the energy levels, but also their lifetimes<sup>4</sup>.

For completeness, we will very briefly outline the main features of this method. The hydrogen Schrödinger equation (including the electric field) in parabolic coordinates can be separated, which allows for high numerical accuracy without too much computational effort. In order to be able to find the energy positions of the resonances as well as their lifetimes, the complex scaling method was applied<sup>25</sup>. Then, for each coordinate the Hamiltonian (including electric field) is expanded with respect to a truncated basis of unperturbed wave functions. This can be done analytically. Finally, the energy levels and lifetimes are obtained by tracking (separately for each level) the eigenvalues of this matrix from zero field in small steps to larger fields.

By using the method described above, we calculated the energies of all states with  $n = 1, 2, 3$  for  $0 \leq \mathcal{E} \leq 0.2$  a.u. The results for the energy levels are depicted in Fig. 3. The levels are labelled by parabolic quantum numbers<sup>26</sup>  $(n_1, n_2, m)$ , which are more suitable for hydrogen in an electric field than the more common spherical quantum numbers  $(n, l, m)$ . The magnetic quantum number  $m$  has the same meaning in both representations. The main quantum number  $n$  is related to the parabolic quantum numbers by  $n = n_1 + n_2 + |m| + 1$ . The electric field lifts all degeneracies except for spin and  $(n_1, n_2, \pm m)$ . So (including spin) there are both two-fold degenerate levels ( $m = 0$ ) and fourfold degenerate levels ( $m \neq 0$ ).

Figure 3 shows that the ground state ( $n = 1$ ) exhibits a small second order shift downwards. The  $n = 2$ -level splits into three levels. Two of them are (for small  $\mathcal{E}$ ) linearly shifting upwards and downwards. The middle one has no first order shift, consistent with the well known results from perturbation theory<sup>26</sup>. Finally, the ninefold

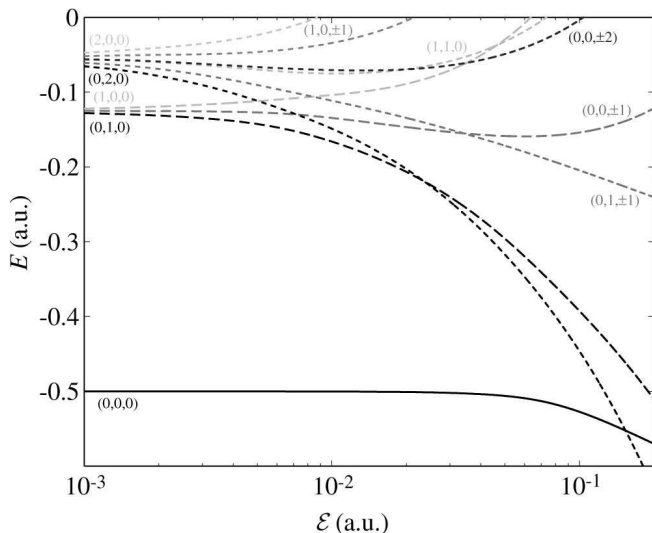


FIG. 3: Evolution of the lowest lying energy levels ( $n = 1, 2, 3$ ) of a hydrogen-like system versus electric field  $\mathcal{E}$ . For conversion of a.u. to conventional units, see Table IV.

degenerate  $n = 3$ -level can be seen to split into six levels. As expected, the effect of the electric field on higher levels is larger, due to their larger spatial extent. At large values of the field, several levels cross each other<sup>36</sup> and some of them show non-monotonous behavior.

The few results of calculations that can be found in literature (obtained by different methods) and overlap with our results are in very good agreement, both for the ground state<sup>6</sup> and for the first excited state ( $m = 1$ )<sup>5</sup>.

The method we used for our calculations can not only be extended to very large fields, but it also has the advantage of yielding the width of the energy levels. The increasing energy width of the hydrogen-like levels in an electric field is the results of the ability of the field to ionize the atom. The finite probability for the carrier to tunnel out of the nucleus' potential well leads to a finite lifetime<sup>37</sup> of the level. In Fig. 4, the evolution of the width of several hydrogen energy levels is depicted. Obviously, the width of all levels is zero at zero field, which is equivalent to an infinitely long lifetime. For any nonzero  $\mathcal{E}$ , the lifetimes have a finite value, that decreases monotonously with the field. The stronger the binding energy of a level at zero field, the faster the lifetime decreases when the field increases.

In Figure 5, the results of Figure 3 and 4 are combined into one 'intensity map', where the levels are displayed as normalized Lorentzian line shapes, the width of which is taken from Fig. 4. The figure shows clearly that for the realistic electric field  $\mathcal{E} = 0.04$  a.u. (about 1 MV/m; see Table IV) the energy width of all levels except the ground state is already larger than or comparable to their binding energy. The ground state lifetime is only 10 ns at that field. We also note that for our purpose it is not very useful to extend the calculation to higher fields, as already at  $\mathcal{E} = 0.2$  a.u. all levels are very much

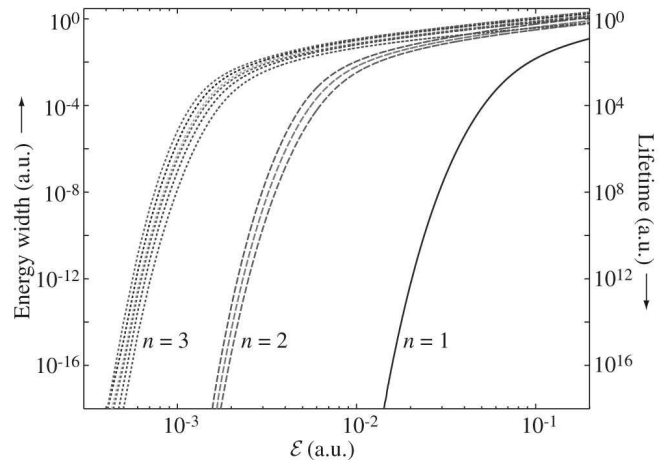


FIG. 4: Energy width and lifetime of the lowest lying energy levels of hydrogen-like systems ( $n = 1, 2, 3$ ) versus electric field  $\mathcal{E}$ . For conversion of a.u. to conventional units, see Table IV.

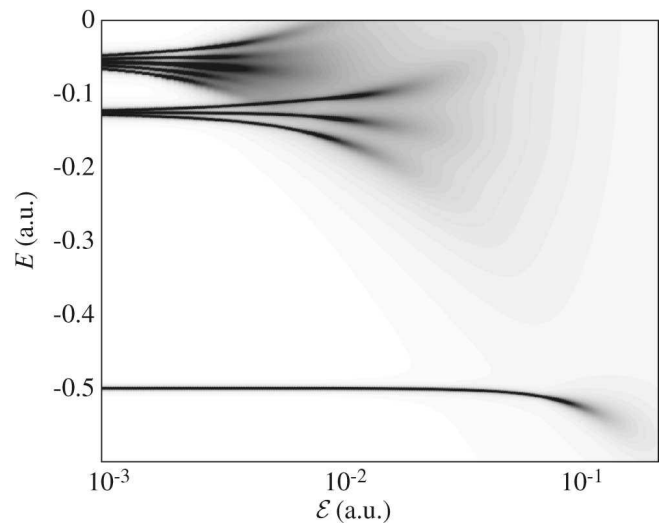


FIG. 5: Map of the energy levels from Figure 3, converted to Lorentzians using the data of Figure 4. For conversion of a.u. to conventional units, see Table IV.

broadened and strongly overlapping. Although in case of hydrogen atoms in vacuum such large field (0.2 a.u.  $\sim 100$  GV/m) are only realized in astronomy, in semiconductors they can be easily achieved under laboratory conditions (0.2 a.u.  $\sim 5$  MV/m).

Though the SHM oversimplifies the bandstructure, it is in our opinion particularly useful to estimate lifetimes. Fig. 4 shows that the lifetimes are primarily a function of the zero-field binding energies. Assuming this is still true when the silicon bandstructure is included, interpolation of the results can be expected to provide a good first order approximation of the level's true lifetime. For example, the  $n = 1$  value in Fig. 4 underestimates the phosphorous donor ground state lifetime, because it is stronger bound than assumed in EMT.



When the electric field is generated by a small local gate, this gate is usually separated from the semiconductor by a potential barrier that is sufficiently high to prevent tunneling. If the distance of the dopant atom to the barrier is not too small, ionization of the dopant atom can still occur in large fields (and the lifetimes discussed before still apply). However, the charge carrier will not be ‘lost’, but transferred to the potential well created by the biased gate<sup>8</sup>.

## V. DISCUSSION AND CONCLUSION

In the preceding sections, we have used two distinct approaches to study the behavior of impurity wave functions in an electric field. The first includes details of the bandstructure, but is only valid for small fields and is somewhat qualitative. From this symmetry-based analysis, we derived the energy level shift and splitting for donors and acceptors in small electric fields, as well as the modification of the donor wave function. Furthermore, the symmetry classification of the resulting levels provides for straightforward prediction of allowed optical transitions.

The second approach, the scaled hydrogen model, is fully quantitative and applicable up to large fields, but neglects most features of the silicon bandstructure. Still, the SHM offers a manageable and valuable way to describe important phenomena in atomic scale electronics. We presented the energy width and lifetime of the impurity levels in large electric fields, calculated within this framework.

It is possible to combine the two approaches and treat Eq. (2) in a way similar to that presented in Section IV. Though this is in principle straightforward, the reduced symmetry and lack of separability will make this approach numerically very involved. Furthermore, it is important to note that the direction of the electric field

with respect to the valley axis is not the same for all valleys. As an example, for  $\mathcal{E} \parallel \mathbf{z}$  the energy levels of  $F_5$  and  $F_6$  are affected in a different way than those of the other four  $F_\mu$ . If the solutions for the various valley wave functions are known, they can be combined into impurity wave functions using the data in Table II.

Though potentially interesting, such an effort is not likely to yield a good description of the dopant’s wave function at high electric fields, despite the tremendous increase of necessary computational power. The reason is the omission of valley orbit interaction, which not only affects the ground state, but also the coupling to excited states. Especially for large fields, the coupling influences the properties *all* energy levels. It has been shown that inter-valley coupling accounts for the splitting of the  $1s$  state for P in Si<sup>27</sup>. Inclusion of this effect appears to be a minimum requirement for obtaining accurate quantitative results valid at large fields.

Recently, calculations of a silicon donor in an electric field in the tight binding approach have been presented<sup>28</sup>. This approach seems to be a useful alternative to calculations based on effective mass theory. Given the fact that this method inherently includes the band structure of the semiconductor host, it is striking how similar the results are to calculations based on the SHM<sup>8</sup>. This underlines the power of the SHM in this type of calculations.

In summary, we have calculated the Stark effect of impurities in silicon in two different approaches. Moreover, we discussed the results and the computation methods used in the context of atomic scale electronics and quantum computation.

## Acknowledgments

One of us, S.R., wishes to acknowledge the Royal Netherlands Academy of Arts and Sciences for financial support.

---

\* Electronic address: g.d.j.smit@tnw.tudelft.nl

† Electronic address: s.rogge@tnw.tudelft.nl

<sup>1</sup> A. Ramdas and S. Rodriguez, Rep. Prog. Phys. **44**, 1297 (1981).

<sup>2</sup> B. E. Kane, Nature **393**, 133 (1998).

<sup>3</sup> B. E. Kane, Fortschr. Phys. **48**, 1023 (2000).

<sup>4</sup> G. Alvarez, R. J. Damburg, and H. J. Silverstone, Phys. Rev. A **44**, 3060 (1991).

<sup>5</sup> F. M. Fernández, Phys. Rev. A **54**, 1206 (1996).

<sup>6</sup> I. A. Ivanov, Phys. Rev. A **56**, 202 (1997).

<sup>7</sup> L. M. Kettle, H.-S. Goan, S. C. Smith, C. J. Wellard, L. C. L. Hollenberg, and C. I. Pakes, Phys. Rev. B **68**, 075317 (2003).

<sup>8</sup> G. D. J. Smit, S. Rogge, J. Caro, and T. M. Klapwijk, Phys. Rev. B (2003), accepted.

<sup>9</sup> A. Fang, Y. C. Chang, and J. R. Tucker, Phys. Rev. B **66**, 155331 (2002).

<sup>10</sup> B. Koiller, X. Hu, and S. D. Sarma, Phys. Rev. Lett. **88**,

027903 (2002).

<sup>11</sup> J. J. White, Can. J. Phys. **45**, 2695 (1967).

<sup>12</sup> A. Köpf and K. Lassmann, Phys. Rev. Lett. **69**, 1580 (1992).

<sup>13</sup> G. M. Guichar, C. Sebenne, F. Proix, and M. Balkanski, Phys. Rev. B **5**, 422 (1972).

<sup>14</sup> K. Larsson and H. G. Grimmeiss, J. Appl. Phys. **63**, 4524 (1988).

<sup>15</sup> W. Kohn and J. M. Luttinger, Phys. Rev. **98**, 915 (1955).

<sup>16</sup> G. Feher, Phys. Rev. **114**, 1219 (1959).

<sup>17</sup> J. M. Luttinger and W. Kohn, Phys. Rev. **97**, 869 (1955).

<sup>18</sup> M. Hamermesh, *Group theory and its application to physical problems* (Addison-Wesley, Massachusetts, 1962).

<sup>19</sup> R. A. Faulkner, Phys. Rev. **184**, 713 (1969).

<sup>20</sup> G. F. Koster, J. O. Dimmock, R. G. Wheeler, and H. Satz, *Properties of the thirty-two point groups* (M.I.T. Press, Cambridge, 1963).

<sup>21</sup> A. K. Ramdas, P. M. Lee, and P. Fisher, Phys. Lett. **7**, 99

- (1963).
- <sup>22</sup> B. S. Tsukerblat, *Group theory in chemistry and spectroscopy*, Theoretical chemistry (Academic press Ltd., London, 1994).
- <sup>23</sup> B. Golding and M. I. Dykman (2003), cond-mat/0309147.
- <sup>24</sup> G. L. Bir, E. I. Butikov, and G. E. Pikus, J. Phys. Chem. Solids **24**, 1475 (1963).
- <sup>25</sup> N. Moiseyev, Phys. Rep. **302**, 211 (1998).
- <sup>26</sup> H. A. Bethe and E. E. Salpeter, *Quantum mechanics of one- and two-electron atoms* (Springer-verlag, Berlin, 1957).
- <sup>27</sup> A. Balderischi, Phys. Rev. B **1**, 4673 (1970).
- <sup>28</sup> A. S. Martins, R. B. Capaz, and B. Koiller (2003), cond-mat/0308575.
- <sup>29</sup> K. Helfrich, Theoret. chim. Acta (Berl.) **24**, 271 (1972).
- <sup>30</sup> In literature discussing donors in silicon, it is more common to denote the single valued representations of  $T_d$  by  $A_1$ ,  $A_2$ ,  $E$ ,  $T_1$  and  $T_2$ , while for acceptors  $\Gamma_i$  ( $i = 1 \dots 5$ ) is used. In this paper, we chose to use the  $\Gamma_i$ -notation in all cases. Moreover, we use the Schönflies symbols to denote the crystallographic point groups<sup>20</sup>.
- <sup>31</sup> It is known from group theory that the reduction of a representation containing more than one instance of the same irreducible representation is not uniquely determined.
- <sup>32</sup> In general, the shift of a  $\Gamma_1$  level cannot have any dependence on the direction of the field.
- <sup>33</sup> Note that a substitutional site in silicon has no inversion symmetry and therefore no definite parity. This is essential for the occurrence of a linear Stark effect in an isolated level.
- <sup>34</sup> In contrast to our treatment of donors, we will use the technique of effective Hamiltonians to derive the matrices for acceptor levels.
- <sup>35</sup> Note that there is a mistake in the corresponding expression in Ref. 24, where the last term between the square brackets is missing.
- <sup>36</sup> Levels belonging to the same representation of the spatial symmetry group  $C_{\infty v}$  can be seen to cross each other in Fig. 3. This is however no violation of the non-crossing rule, since for this specific problem there exists an additional constant of motion that is associated with the separability of the Hamiltonian<sup>29</sup>.
- <sup>37</sup> This lifetime is solely due to the possibility of ionization and is unrelated to (radiative or non-radiative) transitions from an excited level to a lower state.

## APPENDIX A: CHARACTER TABLES

In this appendix, we give for completeness the character tables of various symmetry groups, relevant for this paper. Table V refers to the lattice symmetry group  $\bar{T}_d$ . Depending on the direction of the electric field, it reduces to one of the groups  $C_{2v}$ ,  $C_{3v}$  or  $C_s$ , the character tables of which are given in Table VI. Finally, the table of the continuous groups  $D_{\infty h}$  and  $C_{\infty v}$  are given in Table VII.

TABLE V: Character table for the double group  $\bar{T}_d$ .

	$E$	$\bar{E}$	$8C_3$	$8\bar{C}_3$	$3C_2, 3\bar{C}_2$	$6S_4$	$6\bar{S}_4$	$6\sigma_d, 6\bar{\sigma}_d$
$\Gamma_1$	1	1	1	1	1	1	1	1
$\Gamma_2$	1	1	1	1	1	-1	-1	-1
$\Gamma_3$	2	2	-1	-1	2	0	0	0
$\Gamma_4$	3	3	0	0	-1	1	1	-1
$\Gamma_5$	3	3	0	0	-1	-1	-1	1
$\Gamma_6$	2	-2	1	-1	0	$-\sqrt{2}$	$\sqrt{2}$	0
$\Gamma_7$	2	-2	1	-1	0	$\sqrt{2}$	$-\sqrt{2}$	0
$\Gamma_8$	4	-4	-1	1	0	0	0	0

TABLE VI: Character tables of the single valued irreducible representations of the point groups  $C_{2v}$ ,  $C_{3v}$ , and  $C_s$ .

$C_{2v}$	$E$	$C_2$	$\sigma_v$	$\sigma'_v$	$C_{3v}$	$E$	$2C_3$	$3\sigma_v$	$C_s$	$E$	$\sigma$
$\Gamma_1$	1	1	1	1	$\Gamma_1$	1	1	1	$\Gamma_1$	1	1
$\Gamma_2$	1	-1	1	-1	$\Gamma_2$	1	1	-1	$\Gamma_2$	1	-1
$\Gamma_3$	1	1	-1	-1	$\Gamma_3$	2	-1	0			
$\Gamma_4$	1	-1	-1	1							

TABLE VII: Character table of the groups  $D_{\infty h}$  and  $C_{\infty v}$  (upper left part). These continuous groups have four (two for  $C_{\infty v}$ ) one-dimensional representation and an infinite number of two-dimensional representations. Here  $m$  is a positive integer.

	$E$	$2C_\infty^\varphi$	$\infty\sigma_v$	$i$	$2S_\infty^\varphi$	$\infty C_2$
$\Gamma_g^+$	1	1	1	1	1	1
$\Gamma_g^-$	1	1	-1	1	1	-1
$\Gamma_g^m$	2	$2\cos m\varphi$	0	2	$2\cos m\varphi$	0
$\Gamma_u^+$	1	1	1	-1	-1	-1
$\Gamma_u^-$	1	1	-1	-1	-1	1
$\Gamma_u^m$	2	$2\cos m\varphi$	0	-2	$-2\cos m\varphi$	0